



X-Ray standing waves for investigation of periodic multilayers.

Elena Pavlenko, Moscow State University, Russia.

September 6, 2012

Abstract

Method of X-ray standing waves was realized to investigate the structure of short period multilayer systems. The experiment data was obtained at the E2 bending magnet beamline of DORISII synchrotron radiation source. Fluorescence yield fit was conducted to verify the initial model that was derived from the multilayer growth procedure. The results showed that the original model is not correct and the best consistency between theory and experiment can be received for a model with slight variations of the multilayer periodicity

1.Introduction

X-ray optics - an indispensable tool for the study of various objects. To work with a wavelength (1\AA) used natural crystals with interplanar distance comparable to those wavelengths. X-ray optics is an indispensable tool for the study of various objects. In the case where it is needed a tool for working with a wavelength tens of angstroms of the ultraviolet spectrum - natural crystals are not suitable. In this case layered synthetic microstructures are useful – multilayer with a certain period comparable to the wavelength of interest. [1]

2.Method

2.1 Standing waves

As a fundamental wave phenomenon, the superposition of two coherently coupled X-ray plane-waves localizes the X-ray intensity into interference fringes of an X-ray standing wave (XSW) field (Figure 1). This effect, which is produced by an x-ray reflection, makes it possible to attain a periodic structural probe with a length-scale equivalent to the XSW period [2]:

$$D=(\lambda/2\sin\theta)=2\pi/Q \quad (1)$$

where λ is the X-ray wavelength, 2θ is the scattering angle between the two coherently coupled wave vectors K_R and K_0 , and Q is the scattering vector defined as:

$$Q= K_R-K_0, \quad (2)$$

Q can also be referred to as the standing wave vector, since it points perpendicular to the equal-intensity planes of the XSW and has a magnitude that is the reciprocal of D .

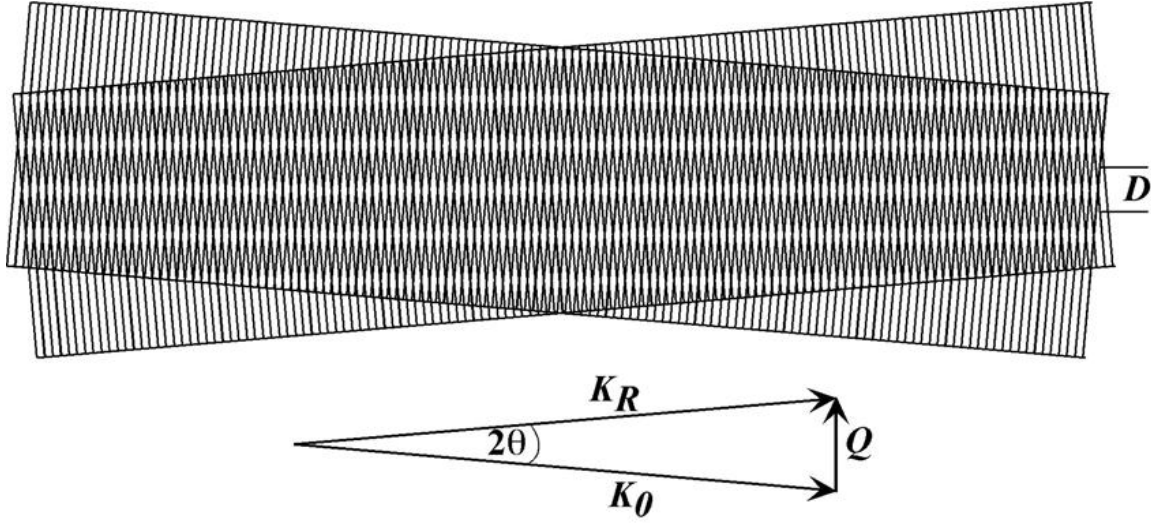


Figure 1. Top: A standing wave field formed from the superposition of two traveling plane waves of wavelength λ and intersection angle (scattering angle) 2θ . The standing wave period is D as defined in Eq. 1. Middle: The two traveling planes waves are represented in reciprocal space by wave vectors K_0 and K_R . $K_0 = K_R = 2\pi/\lambda$. The standing wave is defined by standing-wave vector Q defined in Eq. 2.

2.2 X-Ray standing waves generated by single crystal dynamical Bragg diffraction.

The most commonly used means for generating an X-ray standing wave is the use of strong Bragg diffraction from a single-crystal. In 1964, using Bragg diffraction from a Ge crystal, Batterman (1964) made the first observation of the XSW effect—an angularly modulated Ge fluorescence yield across the reflection. Later, Golovchenko and coworkers realized that the XSW field generated inside the crystal extended above the crystal surface and used the XSW to determine the crystallographic registration of adsorbate atoms with respect to the underlying substrate lattice (Cowan et al. 1980; Golovchenko et al. 1982).

Method of XSW is well developed for single crystals. The creation of a standing wave is due Periodicity of atomic planes of the crystal. This method is

also suitable for the study of multilayer where layers of materials with different densities play the role of atomic planes. Then, the theory of standing waves for single crystals is similar to multilayer.

An X-ray standing wave generated by single crystal Bragg diffraction can be used to determine the 3D lattice location of bulk impurity atoms and surface adsorbents. Dynamical diffraction theory, which solves Maxwell's equations in a periodic dielectric with appropriate boundary conditions, is used to describe the fields inside and outside of the crystal.

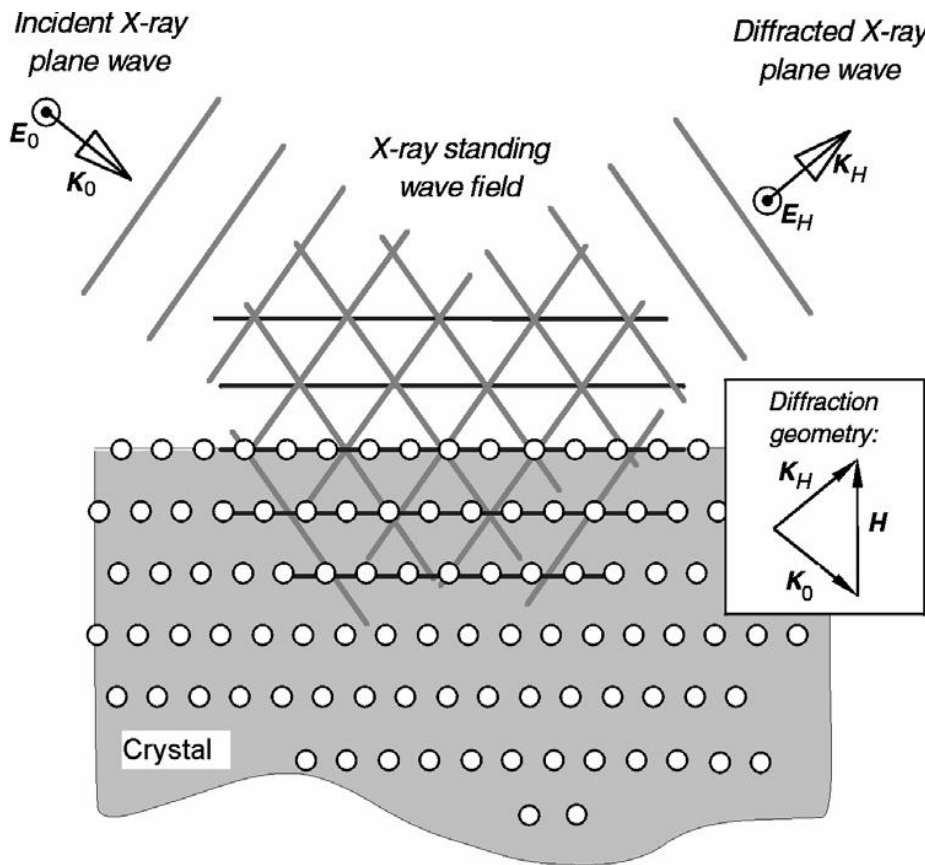


Figure 2. X-ray standing wave field formed in a crystal and above its surface by the interference of incident and Bragg-diffracted X-ray plane waves. The XSW period is equal to the d spacing “ d ”. Aligning a XSW nodal (or antinodal) plane with an atomic plane will minimize (or maximize) the characteristic fluorescence yield from that atomic plane.

2.3 Theory

Consider the two-beam Bragg diffraction condition, described in Figure 2 , where the incident and the Bragg-diffracted X-ray plane waves are expressed as:

$$\begin{aligned}\mathcal{E}_0(\mathbf{r}, t) &= E_0 \exp[-i(K_0 \cdot \mathbf{r} - \omega t)] \\ \mathcal{E}_H(\mathbf{r}, t) &= E_H \exp[-i(K_H \cdot \mathbf{r} - \omega t)]\end{aligned}\tag{3}$$

Here E_0 and E_H are the complex amplitudes associated with the incident and diffracted X-ray plane-waves, K_0 and K_H are the respective complex wave vectors inside the crystal, and ω is the X-ray frequency. The two wave vectors are coupled according to the Laue condition:

$$\mathbf{H} = \mathbf{K}_H - \mathbf{K}_0\tag{4}$$

where $\mathbf{H} = h\mathbf{a}^* + k\mathbf{b}^* + l\mathbf{c}^*$ is a reciprocal lattice vector. The scalar equivalent of the Laue condition reduces to Bragg's law,

$$\lambda = 2d_H \sin \theta_B$$

where $d_H = 2\pi/|\mathbf{H}|$ is the lattice spacing of the $\mathbf{H} = hkl$ crystal diffraction planes and θ_B is the geometrical Bragg angle. The interference between the incident and diffracted plane waves results in a standing-wave field. The normalized intensity of the total E-field that gives rise to the XSW field is

$$\begin{aligned}I(\theta, r) &= \frac{|\mathcal{E}_0 + \mathcal{E}_H|^2}{|E_0|^2} \\ &= \left[1 + R(\theta) + 2\sqrt{R(\theta)} \cos(\nu(\theta) - \mathbf{H} \cdot \mathbf{r})\right] \times \begin{cases} 1 & ; \text{ above the surface} \\ e^{-\mu_c(\theta)z} & ; \text{ at depth } z \text{ below surface,} \end{cases}\end{aligned}\tag{5}$$

where the reflectivity R is related to the E -field amplitude ratio as:

$$R = \left| \frac{E_H}{E_0} \right|^2 \quad (6)$$

and the XSW phase, ν , is identical to the relative phase between the two E-field amplitudes,

$$\frac{E_H}{E_0} = \left| \frac{E_H}{E_0} \right| \exp(i\nu) \quad (7)$$

From Equations (1) and (5), one can conclude that for Bragg diffraction the XSW periodicity is equal to the lattice d -spacing of the $H = hkl$ diffraction planes; that is, $D = dH$. In the following discussion, we will assume the most common case of σ -polarized symmetrical Bragg diffraction from a semi-infinite crystal with $1^\circ < \theta < 89^\circ$. Figure 2 shows the case of σ -polarization with the vector directions of the two E -fields pointing perpendicular to the scattering plane defined by the two wave vectors. The incident and exit angles of the two wave vectors with respect to the surface are equivalent for a symmetric reflection.

From dynamical diffraction theory (Batterman and Cole 1964), the E -field amplitude ratio is defined as [3]

$$\frac{E_H}{E_0} = -\sqrt{\frac{F_H}{F_{\bar{H}}}} \left(\eta \pm \sqrt{\eta^2 - 1} \right) \quad (8)$$

Where F_H and $F_{\bar{H}}$ are the H and $-H$ structure factors, which describe the superposition of the coherent x-ray scattering from the N atoms within the unit cell as:

$$\begin{aligned} F_H &= |F_H| \exp(i\phi_H) \\ &= \sum_{n=1}^N \left[f_n^0(H) + \Delta f_n'(\lambda) + i \Delta f_n''(\lambda) \right] s_n(H) \mathcal{D}_n(H) , \end{aligned} \quad (9)$$

Where $s_n(H) = \exp(iH \cdot r_n)$ is the geometrical phase factor for the n^{th} atom located at r_n relative to the unit cell origin. $\mathcal{D}_n(H) = \exp(-M_n)$ is the Debye-Waller temperature factor for the n^{th} atom. $\Delta f_n'$ and $\Delta f_n''$ are the real and imaginary

wavelength dependent anomalous dispersion corrections to the atomic form factor f_n^0 (H). η is the normalized angle parameter defined as:

$$\eta = \frac{-\Delta\theta \sin(2\theta_B) + \Gamma F_0}{\Gamma \sqrt{F_H F_{\bar{H}}}} \quad (10)$$

In this equation, $\Delta\theta = \theta - \theta_B$ is the relative incident angle. $\Gamma = (r_e \lambda^2) / (\pi V_c)$ is a scaling factor, $r_e = 2.818 \times 10^{-5}$ Å is the classical electron radius and V_c is the volume of the unit cell. (To separate the real and the imaginary parts of a complex quantity A , the notation $A = A' + iA''$ is used, where A' and A'' are real quantities.) From Eq. (6-10) it can be shown that the reflectivity approaches unity over a very small arc-second angular width w , defined as:

$$w = \Delta\theta_{\eta'=-1} - \Delta\theta_{\eta'=1} = \frac{2\Gamma \sqrt{F'_H F'_{\bar{H}} + F_0'^2 - F''_H F''_{\bar{H}}}}{\sin 2\theta_B} \quad (11)$$

This is the “Darwin width” of the reflectivity curve or “rocking curve”. Using the above dynamical diffraction theory equations (Eq. 7-10), one can show that the relative phase, ν , of the standing wave field decreases by π radians as the incident angle is scanned from the low-angle side to the high-angle side of the rocking curve. According to Eq. (5), this causes the standing-wave antinodal planes to move by a distance of $\frac{1}{2}d_H$ in the $-\mathbf{H}$ direction. Also from Eq. (5), if $\Delta f_n'' = 0$, then $R=1$, and the intensity at the antinode is four-times the incident intensity, $|E_0|^2$ and there is zero intensity at the node. The case of $I = 4$ at the antinode assumes that the field is being examined above the surface or at a shallow depth where $\exp(-\mu_z z) \approx 1$. The Darwin width, w , is dependent on both the structure factors and the wavelength of the incident X-ray beam. For a typical low-index strong Bragg reflection from a inorganic single crystal w is within the range of 5 to 100 micro radians (μrad) for X-rays within the range of $\lambda = 0.5$ to 2 Å.

The exponential damping factor in Eq. (5) accounts for attenuation effects within the crystal, in which case the effective absorption coefficient is defined as:

$$\mu_z(\theta) = \frac{\mu_0}{\sin \theta_B} \left[1 + \frac{F'_H}{F_0''} \left(\frac{E_H}{E_0} \right)'' + \frac{F''_H}{F_0''} \left(\frac{E_H}{E_0} \right)' \right], \quad (12)$$

Where $\mu_0 = \frac{2\pi}{\lambda} F_0''$ is the linear absorption coefficient. The second and third terms in Eq. (12) account for the extinction effect that strongly limits the X-ray penetration depth $1/\mu_z$ for a strong Bragg reflection. For example, the penetration depth for 15-keV X-rays at the GaAs (111) Bragg reflection goes from 2.62 μm at off-Bragg conditions to 0.290 μm at the center ($\eta' = 0$) of the Bragg rocking curve. The general expression for this minimum penetration depth or extinction length is:

$$\Lambda_{ext} = V_c [4d_H r_e (F_0'' + \sqrt{|F_H| |F_H|})]^{-1} \quad (13)$$

2.4 Secondary processes in case of X-ray standing wave.

The XSW field established inside the crystal and above the crystal surface induces different secondary processes. The excited ions, in turn, emit characteristic fluorescence X-rays and Auger electrons. For the discussion that follows, we will assume the dipole approximation, in which case the normalized X-ray fluorescence yield is defined as:

$$Y(\theta) = \int I(\theta, r) \rho(r) \exp[-\mu_f(\alpha) z] dr \quad (14)$$

where $\rho(r)$ is the normalized fluorescent atom distribution, and $\mu_f(\alpha)$ is the effective absorption coefficient for the emitted fluorescent x-rays which is dependent on their takeoff angle, α . Upon integration, the normalized XSW yield is given as:

$$Y(\theta) = [1 + R(\theta) + 2\sqrt{R(\theta)} f_H \cos(v(\theta) - 2\pi P_H)] Z(\theta) \quad (15)$$

where the parameters f_H and P_H are the coherent fraction and coherent position, respectively. In more general terms, f_H is the amplitude and P_H is the phase of the H^{th} order Fourier coefficient of the normalized distribution function:

$$\mathcal{F}_H = \int_{uc} \rho(\mathbf{r}) \exp(i\mathbf{H} \cdot \mathbf{r}) d\mathbf{r} = f_H \exp(2\pi i P_H) \quad (16)$$

$Z(\theta)$ is the effective-thickness factor, which will be discussed below. $Z(\theta) = 1$ for atoms above the surface of the crystal and at a depth much less than the extinction length, $Z(\theta) \sim 1$.

2.5 X-Ray standing waves from layered synthetic periodic multilayers.

For Bragg diffraction purposes, a layered-synthetic microstructure (LSM) is fabricated (typically by sputter deposition) to have a depth-periodic layered structure consisting of 10 to 200 layer pairs of alternating high- and low-electron density materials, such as Mo and Si. Sufficient uniformity in layer thickness is obtainable in the range between 10 and 150 Å (d -spacing of fundamental diffraction planes from 20 Å to 300 Å). Because of the rather low number of layer pairs that affect Bragg diffraction, these optical elements (when compared to single crystals) have a significantly wider energy band pass and angular reflection width. The required quality of a LSM is that experimental reflection curves compare well with dynamical diffraction theory, and peak reflectivity's are as high as 80%. Therefore, a well-defined XSW can be generated and used to probe structures deposited on an LSM surface with a periodic scale equivalent to the rather large d -spacing. To a good approximation, the first-order Bragg diffraction planes coincide with the centers of the high-density layers of the LSM. Above the surface of the LSM, the XSW period is again defined by Eq. (1). The reflectivity can be calculated by using Parratt's recursion formulation. This same optical theory can be extended to allow the calculation of the E -field intensity at any position within any of the slabs over an extended angular range that includes TER.

Equal

$$Y(\theta) = \int_{z=0}^{z=\infty} I(\theta, z) \rho(z) dz \quad (17)$$

is used to calculate the fluorescence yield. The LSM-XSW method is primarily used to determine atom (or ion) distributions in deposited organic films or at electrified liquid/solid interfaces.

2.6 Modeling

At first the distribution of the electromagnetic field was calculated by using a model of this structure which was described at figure 1. For creating the model of electromagnetic field the webs interface TER_SL [5]. The results of modeling are shown in figure 4 a). This graph shows the distribution of the field as a function of depth and angle. Using this distribution it is possible to model the intensity of the fluorescence yield for a given crystal thickness. Depending on the depth at which the layer of La – curve of fluorescence will be different – it is possible to see a phase changes. Figure 4 b) shows this.

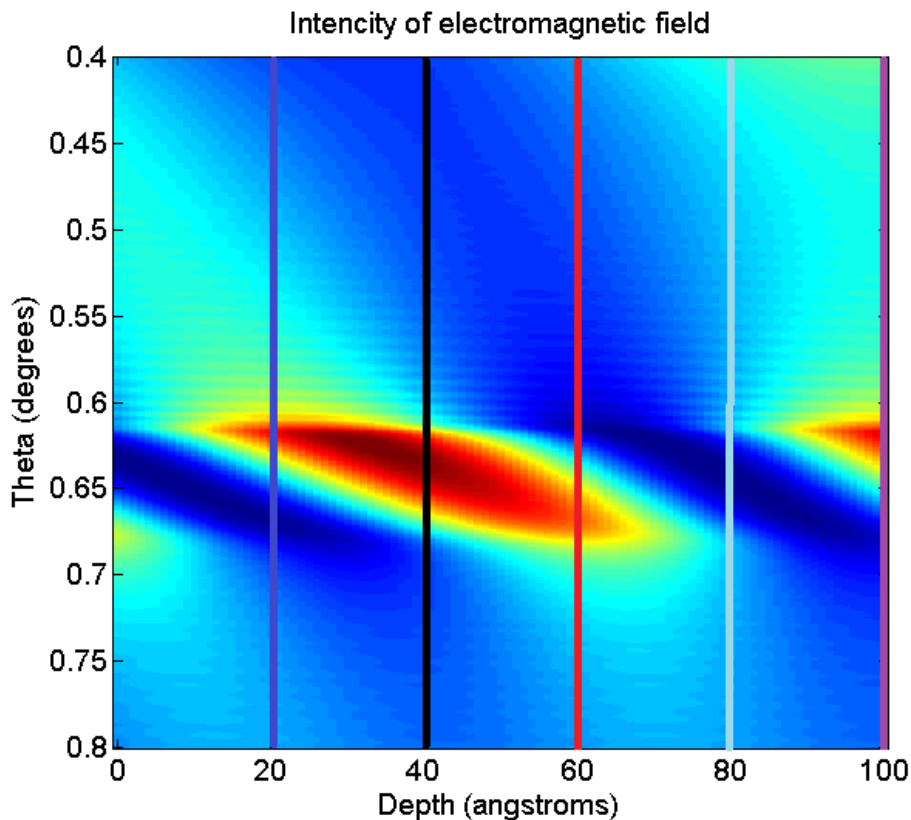


Figure 4 a)

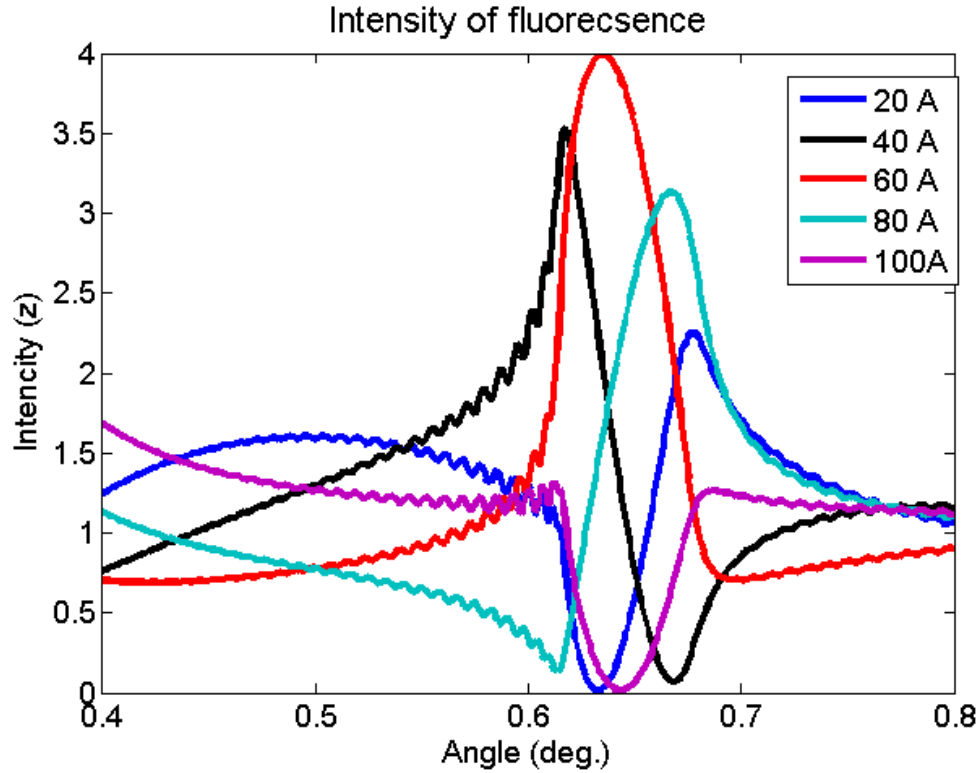


Figure 4 b)

Figure 4. a) The distribution of the field in depth and in angle. b) Fluorescence yield from different depths.

3 Experiment

3.1 Object

We have investigated the multilayer structure Mo/B -grown on the Si substrate. Multilayer was deposited on super polished silicon substrates with a modified DC magnetron sputtering system, using the setup described in ref. [4]. Magnetron sputtering deposition is a process where plasma of ions is attracted to the target containing the material that is to be sputtered. The material will vaporize, when these energetic ions hit the target. As a sputter gas Ar was used. Ar pressure was about 10^{-4} mbar. Layer thickness was controlled by fixing the time of layer deposition. Quartz crystals are used to measure the amount of deposited material.

The sample holder is rotated during sample fabrication to average any non-uniformity in the vapor flux. The multilayer stack consists of 50 layer pair of Mo and B with thickness of 14\AA and 20\AA , correspondently. On the top of multilayers wear formed lanthanum thin film 3\AA , surrounded by 20\AA carbon layers. Schematic drawing of sample cross section are shown on the figures below.

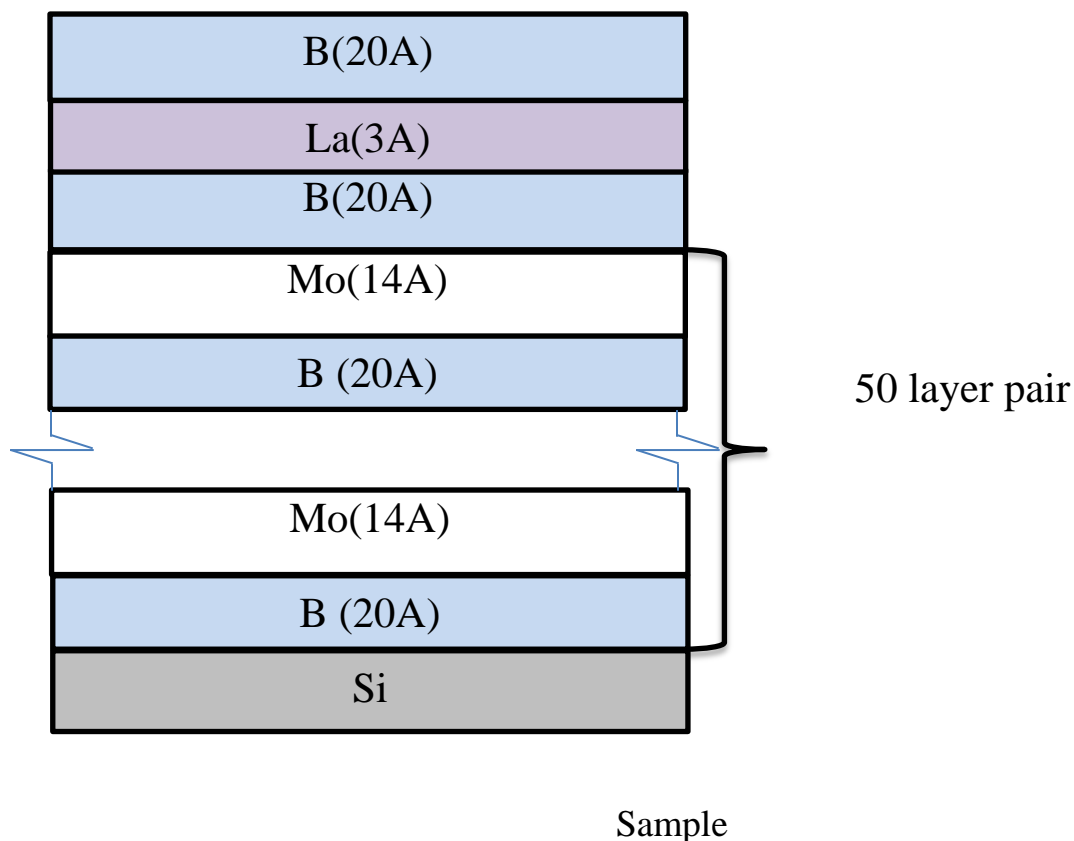


Figure. 1 Schematic drawing of the sample with thickness of La 3\AA .

3.2 Measurements

X-ray reflectivity curves were measured on the PANAnalytical Expert Pro diffractometer, which was equipped with 2 kWt X-ray tube. CuK x-ray radiation was prepared using an asymmetrical cut 4 crystal monochromator 4xGe(220). The direct beam intensity was $3.5 \cdot 10^6$ c.p.s. with an angular divergence of around

0.01°. The sample was scanned in the θ -2 θ mode with an angular step of 0.005° with an exposure time of two seconds at each point. Such an experimental setup allowed for the measurement of six orders of diffraction peaks with a deflection of less than nine degrees. From these peaks it was possible to resolve the thickness oscillations.

The measurement of the X-ray standing waves was performed at the E2 beamline of DORISII synchrotron radiation source. Synchrotron radiation selection and monochromatization was carried out using a double crystal monochromator of Si (111). Such an experimental scheme provides the energy resolution $\Delta\lambda/\lambda = 5 \cdot 10^{-4}$. X-ray radiation with an energy of 8 keV - above L-absorption edge of La - was used in the experiments. X-ray reflectivity curves were measured in the area of the Bragg peak in θ -scan mode with a point detector – pin-diode. After standing waves of X rays were formed at the Bragg angle in the crystal, secondary fluorescence from the La $L_{\alpha,\beta,\gamma}$ lines were observed using the energy dispersive detector Ketek-SDD.

The reflectivity curves from the layers contain a series of diffraction peaks and the interference oscillations between them. Figures 6 show the fluorescence yield distribution (green) and the Bragg peak. For the visualization of the fluorescence measurements two curves are shown - the fluorescence yield curve and the peak of Bragg reflection.

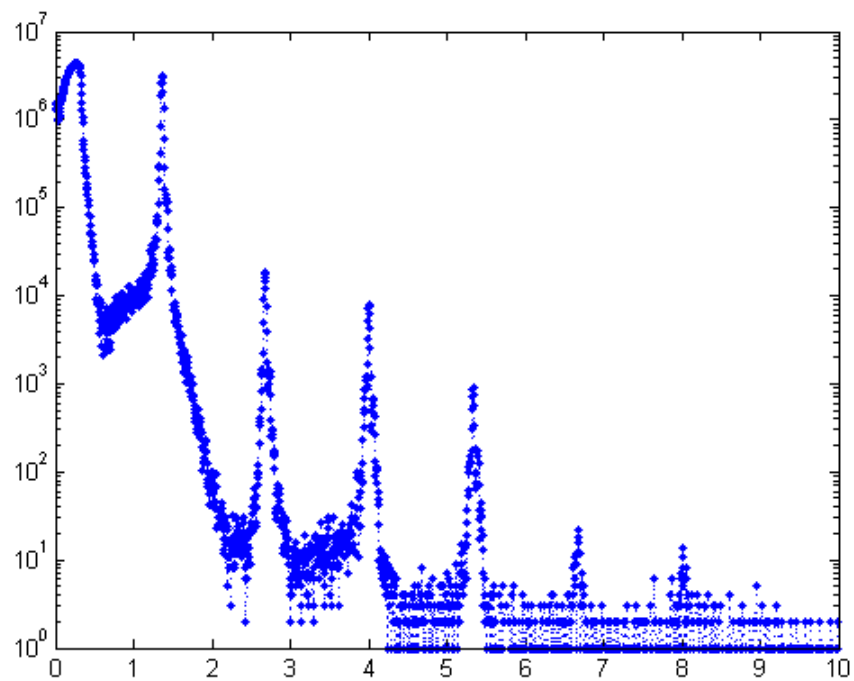


Figure 5. X-ray reflectivity curve, from the sample

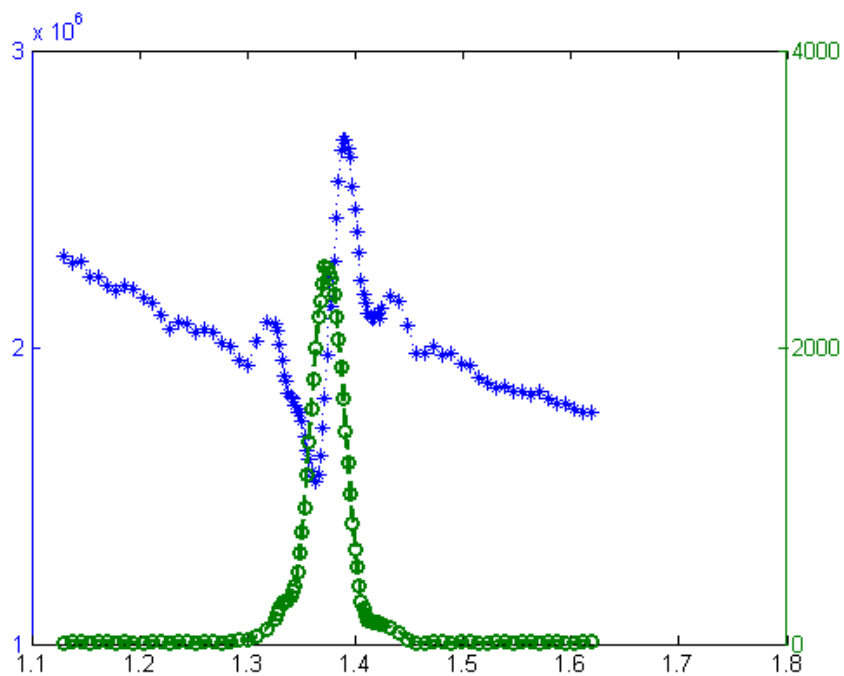


Figure 6. Experimental fluorescence yield (+, blue curve) and the peak of Bragg reflection (o, green curve)

4 Analysis and results

To obtain the information about the structure, the standard procedure of fitting theoretical curves to the experimental data was used. The procedure was repeated using a range of different model parameters. Each repeating unit of the crystal structure is comprised of two layers one Mo and one B. Each layer has a characteristic thickness, complex refractive index and roughness of the border. Providing the multilayer crystal is of high quality, every unit repeating unit of the multilayer structure can be assumed to be equivalent. The advantage of this assumption is that it reduces the number of free parameters. The degree of convergence of the experimental data with the theoretical model is evaluated using the parameter χ^2 (goodness of fit). This parameter allows for a combination of the statistical errors at each point, bias. The χ^2 value is given by the following equation:

$$\chi^2 = \frac{1}{n - N_p} \sum_{j=1}^n \frac{(I_j^{exp} - I_j^{calc})^2}{s_j^2}$$

Where n is the number of data points, N_p is the number of unknown parameters, I_{exp} and I_{calc} are the measured and calculated theoretical intensity and s_j is the statistical error.

After processing the reflectivity data, the chi squared was 9.7 which is a very good criterion of agreement between theory and experiment. Figure 8 shows that the angular position of all reflexes is correct, as there is no divergence in intensity. Based on these parameters (position and intensity of the Bragg's peaks) it is possible to estimate the average value of the period of the structure and the electron density profile. These results imply that our model and assumptions are correct.

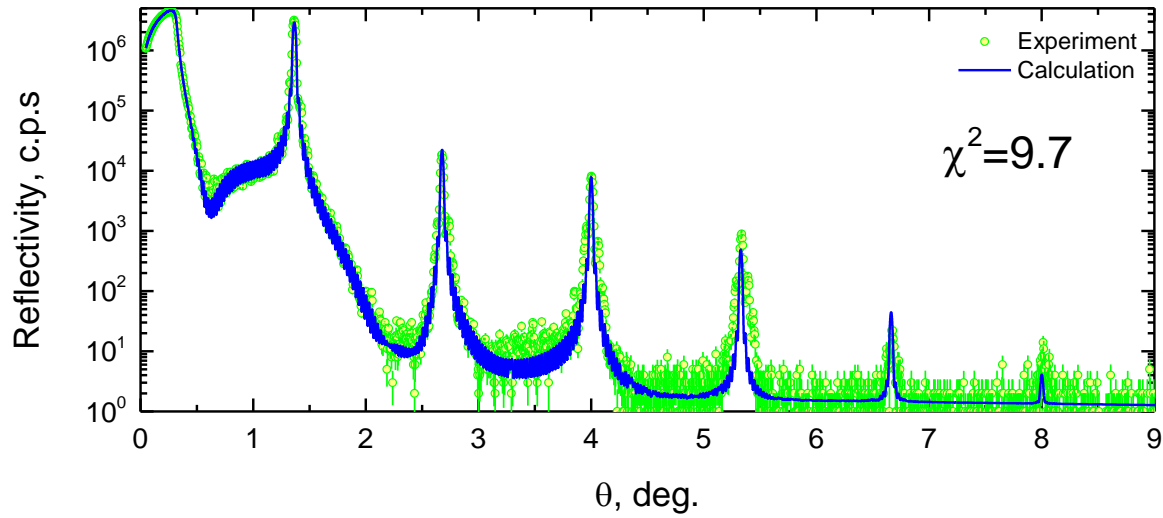


Figure 8. Fit of the reflectivity curve from sample 1.

There is a table below. This table shows the parameters of the model have been derived from the fit.

	Thickness (Å)	Roughness/2 (Å)	Density (g/cm ³)	Amount of B	Amount of La
Bo/La/Bo	48.70691850	4.59210745	3.78403954	8.04172286	1.27409809
Mo	17.55525864	2.29001364	7.98096333		
B	15.67402502	3.94205624	2.73193217		
Si					

Electromagnetic field in the sample was calculated using the model of the specimen obtained during the fit. The theoretical curve of the fluorescence yield is calculated from the field pattern, and then the procedure is to fit a theoretical model of experimental data of the fluorescence yield. Results are shown in Figure 9.

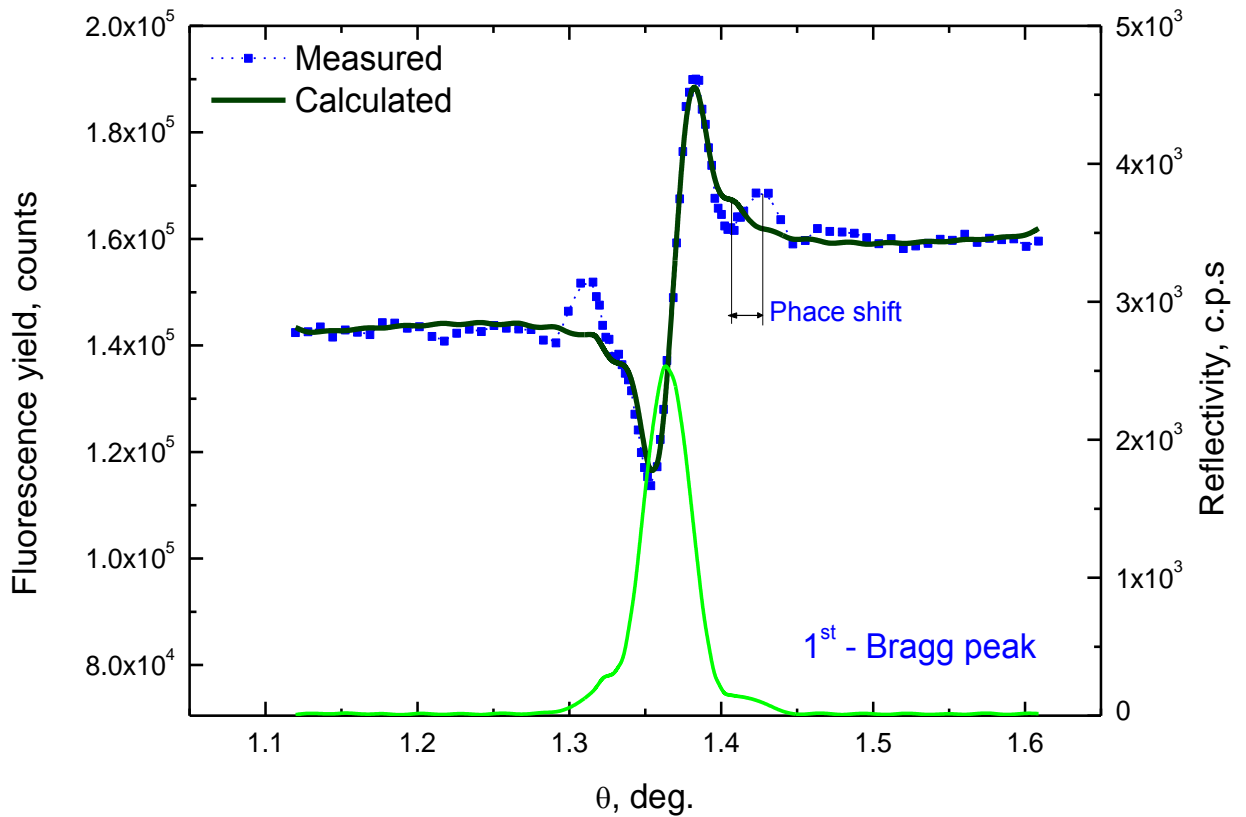


Figure 9. Fit of the fluorescence yield from sample.

It can be seen that the curve calculated theoretically describe oscillations in the tails are not very good. In this case, the convergence of theory and experiment is not satisfactory. This fact indicates that the calculated model is not correct.

On the curve of reflectometry this defect may affect the oscillations of the thickness, which are situated between the Bragg peaks. Indeed, if you look at the details of reflectometry curve fit, you can see the discrepancy between theory and experiment in the area of the curve. Figure 10.

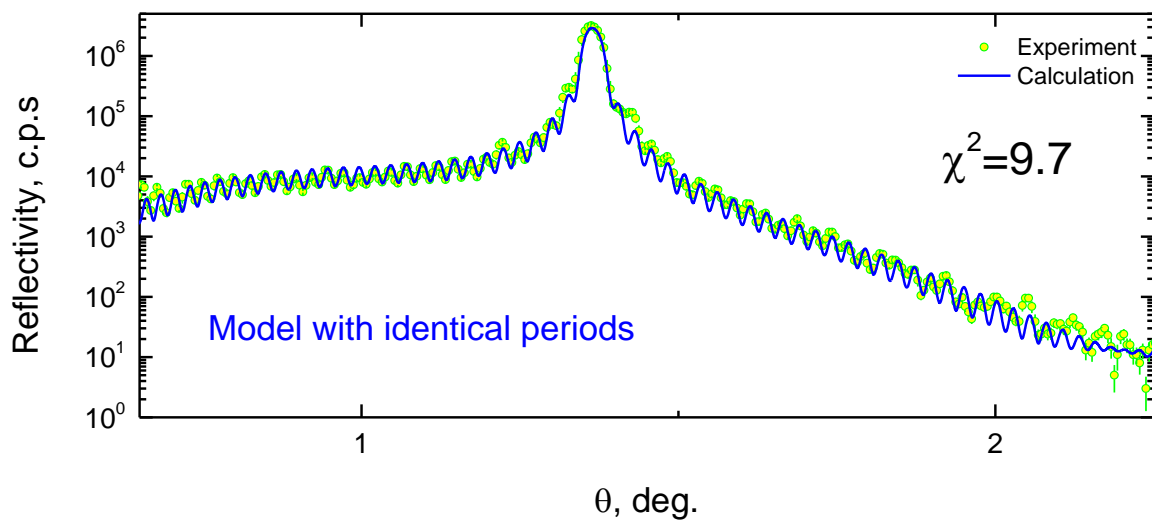
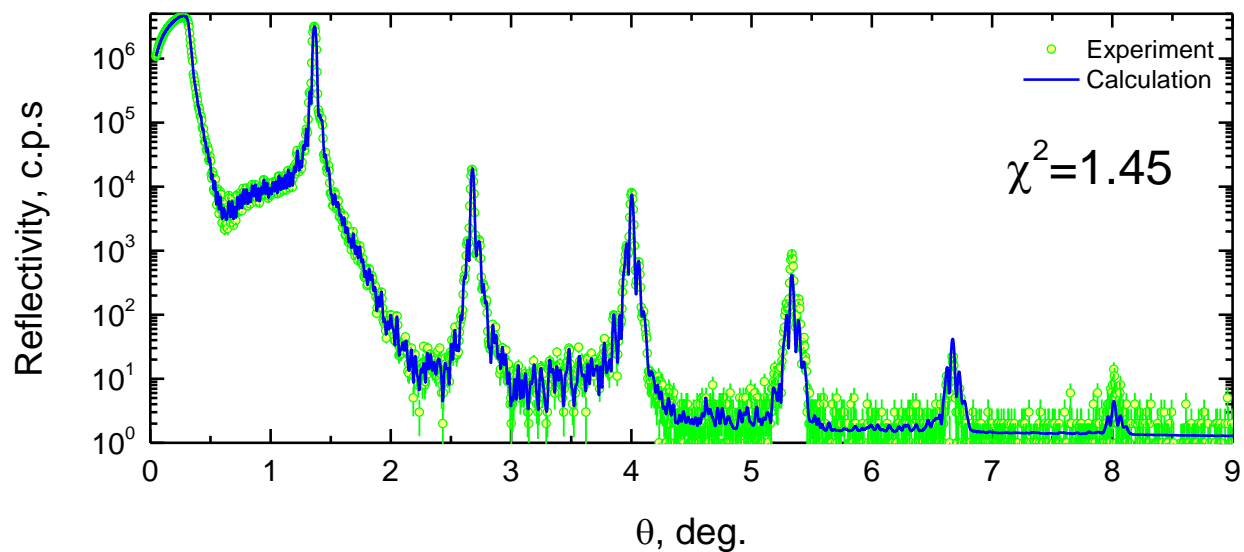


Figure 10. Fit of the reflectivity curve from sample 1 in range of first Bragg's peak.

Therefore it possible to conclude that the assumption of the identity of the layers was not valid and should be considered each layer independently. Below are the results of the second fit with the possible differences of each layer of multilayer structure. Now the parameter χ^2 was even less evidence that agreement between theory and experiment is much better. Figure 11. a), b).



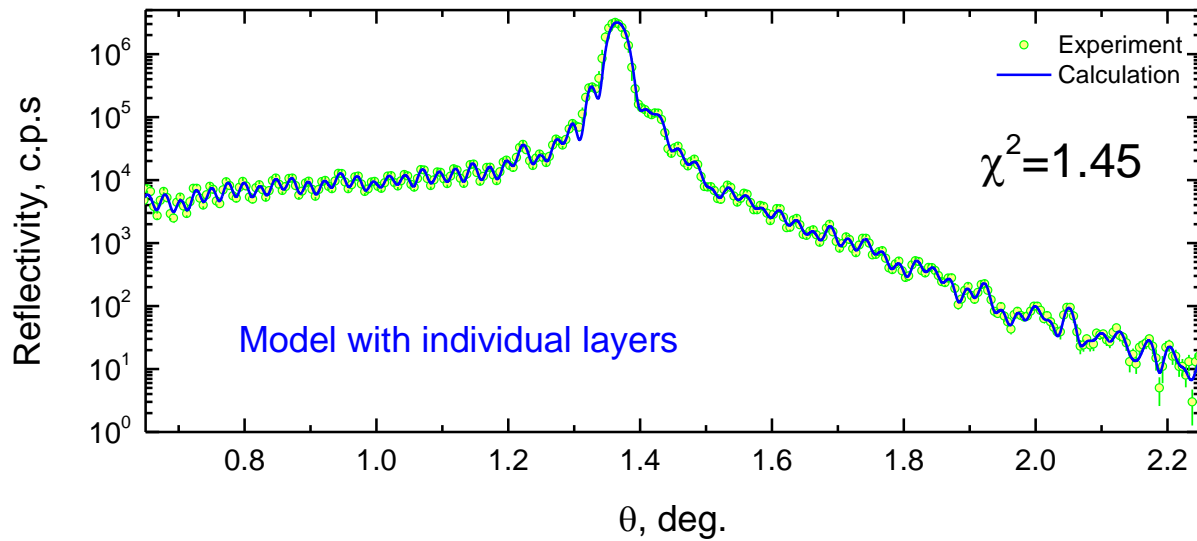


Figure 11. Fit of the reflectivity curve, Bragg's peak.

a) Whole data b) in range of first.

This table shows the parameters of the model have been derived from the fit.

	Mean thickness (Å)	Mean roughness (Å)	Mean density (g/cm ³)	Amount of B	Amount of La
Bo/La/Bo	48.4454	4.6295	3.7283	8.0417	1.2740
Mo	17.5314± 0.2293	2.2203±0.2393	7.8856±0.3403		
B	15.7200± 0.2614	3.7739±0.2683	2.7189±0.4220		
Si					

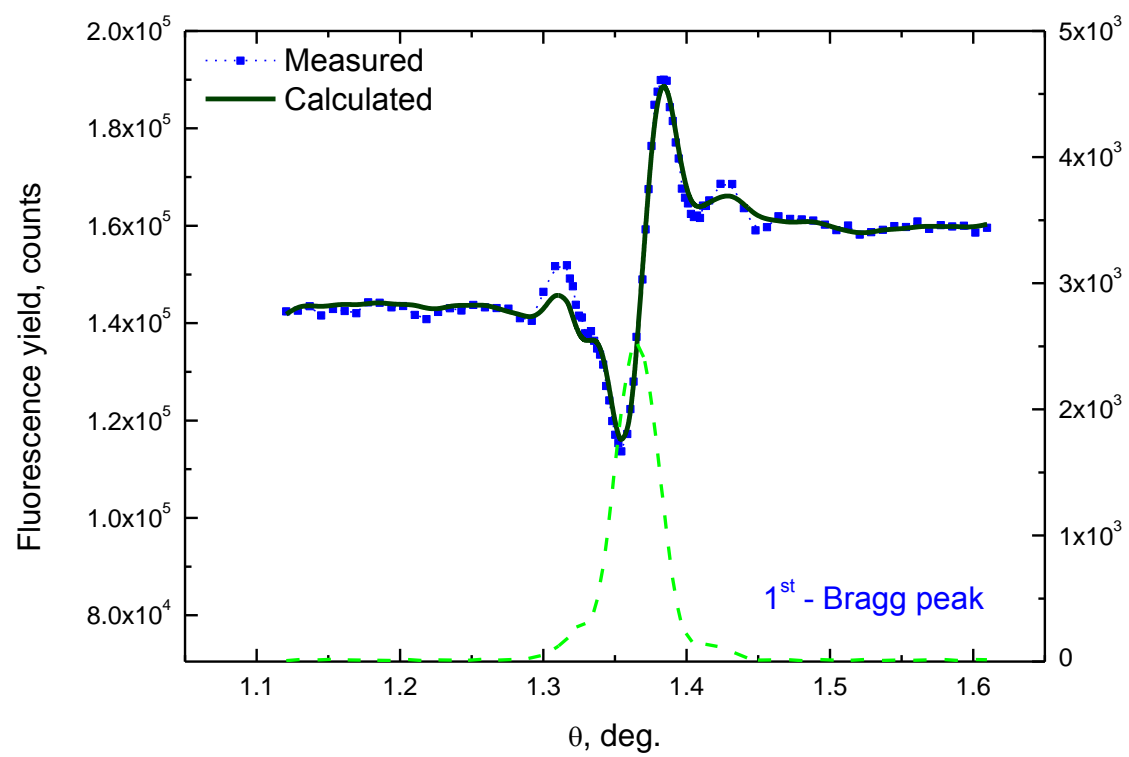


Figure 12. Fit of the fluorescence yield.

5. Conclusions

1) X-ray standing wave method has been implemented for the analysis of multilayer.

2) The model structure proposed by deposition team has been in checked.

3) The model of the investigated multilayer structure which correctly describes the investigated multilayer structure was created. This model is based on the analysis of the measured data.

4) It is shown that the method of X-ray standing waves can be successfully used for analysis of multilayer structure.

5) In this work X-ray standing waves method was realized for the object with subsidiary thin layer of La.

6) Investigation of applying this method for other object, also with thick subsidiary layers is continuous.

6. References

- [1] Michael J. Bedzyk and Likwan Cheng, "X-ray Standing Wave Studies of Minerals and Mineral Surfaces: Principles and Applications" (Reviews in Mineralogy and Geochemistry, Vol. 49), Geochemical Society 221-266 (2002).
- [2] Afanas'ev AM, Kohn VG (1978) External photoeffect in the diffraction of X-rays in a crystal with a perturbed layer. Sov Phys JETP 47: 154-161
- Takahashi T, Kikuta S (1979) Variation of the yield of photoelectrons emitted from a silicon single crystal under the asymmetric diffraction condition of X-rays. J Phys Soc Japan 46:1608-1615
- Hertel N, Materlik G, Zegenhagen J (1985) X-ray standing wave analysis of Bi implanted in Si(110). Z Phys B 58:199-204
- Bedzyk MJ and Materlik G (1985) Two-beam dynamical diffraction solution of the phase problem: A determination with X-ray standing waves. Phys Rev B 32:6456-6463
- Zegenhagen J (1993) Surface structure determination with X-ray standing waves. Surf Sci Rep18:199-271
- Laue M (1960) Roentgenstrahl-Interferenzen, Akademische-Verlagsgesellschaft, Frankfurt
- Authier A (2001) Dynamical Theory of X-ray Diffraction. Oxford University Press, New York
- [3] Batterman BW, Cole H (1964) Dynamical diffraction of X-rays by perfect crystals. Rev Mod Phys 36:681-717
- [4] Yakshin, A.E., et al., Enhanced reflectance of interface engineered Mo/Si multilayers produced by thermal particle deposition. Proc. of SPIE 2007. 6517: p. 65170I-1 - 65170I-9.
- [5] Used web interface available at <http://sergey.gmca.aps.anl.gov/>

